



Microstructure, morphology, and methylene blue degradation over nano-CuFe₂O₄ synthesized by a modified complexometric method

Mrinal Saha¹ · Arup Gayen² · Siddhartha Mukherjee¹

Received: 17 March 2017 / Revised: 9 October 2017 / Accepted: 12 January 2018 / Published online: 13 February 2018
© Australian Ceramic Society 2018

Abstract

Nanodimensional copper ferrite has been successfully synthesized via a modified complexometric method using ethylenediaminetetraacetic acid and citric acid as the complexing agent and the fuel, respectively. The physical and chemical behaviors of this spinel ferrite material have been explored by using different kinds of techniques including thermogravimetric analysis/differential scanning calorimetry (TGA/DSC), X-ray diffraction (XRD), field emission scanning electron microscopy (FE-SEM), atomic force microscopy (AFM), high-resolution transmission electron microscopy (HR-TEM), vibrating sample magnetometry (VSM), and N₂ adsorption–desorption isotherm. The crystallite size falls in the range 13–30 nm depending on the calcination temperature required for phase formation. The surface morphology of the polycrystalline ferrite material is almost spherical. The band gap value and BET-specific surface area are determined to be 1.40 eV and 32 m² g⁻¹, respectively. This spinel ferrite behaves as a mesoporous (2–50 nm) material, and the material formed at a higher calcination temperature has agglomeration tendency. The CuFe₂O₄ exhibits typical soft ferromagnetic behavior with saturation magnetization value of 52 emu g⁻¹. Of interest, it has the capability to degrade 96% of methylene blue in acidic medium (pH = 4) in 45 min under the visible light in presence of H₂O₂ as oxidant.

Keywords Nanodimensional-CuFe₂O₄ · Modified complexometric method · Mesoporous material · Spherical morphology · Methylene blue degradation · Ferromagnetic

Introduction

Over the last decades, nanostructured spinel ferrite (MFe₂O₄) materials have drawn considerable attention of the researchers of materials chemistry and physics due to their unique physical and chemical properties [1]. Copper ferrite is one of the important materials belonging to the fascinating class of spinel ferrites because it exhibits phase transitions, changes in semi-conducting properties, and shows electrical switching and tetragonality variation when treated under different conditions in addition to interesting magnetic and electrical properties with chemical and thermal stabilities [2]. It is used in the wide

range of applications in gas sensing, catalytic applications, Li ion batteries, high-density magneto-optic recording devices, color imaging, bioprocessing, magnetic refrigeration, and ferrofluids [2–8]. Nanosized copper spinel ferrite shows unusual properties in comparison with their bulk analogs and received enormous attention due to their potential applications. At the same time, these well-established properties of spinel ferrites crucially depend on the synthesis methods [9].

Several physical and chemical methods have been developed for the synthesis of copper ferrite including solid-state reaction, solution combustion, sol–gel, coprecipitation, mechano-chemical method, polyol route, microemulsion, and hydrothermal route [10–15]. These methods have several advantages as well as some disadvantages. The major disadvantage of the microemulsion route is its low production rate, and it is also costly. The solid-state reaction and mechano-chemical methods are both energy and time consume processes. In the case of sol–gel technique, time consumption and costing are the main challenging factors. In the coprecipitation method, sometimes impurities are formed along with the desired material. However, complexometric process is an

✉ Mrinal Saha
mrinalsaha2009@gmail.com

¹ Department of Metallurgical & Material Engineering, Jadavpur University, Kolkata 700032, India

² Department of Chemistry, Jadavpur University, Kolkata 700032, India

efficient method for the preparation of metal oxide material in their nanodimension. The attractive features of complexometric process are its ability to synthesize materials with high purity, better homogeneity, and high surface area in a single step. Recently, Yan et al. studied complexometric route to synthesis irregular CuFe_2O_4 nanoparticle using ethylenediaminetetraacetic acid (EDTA) as a chelating agent [16]. Tu and coworkers synthesized CuFe_2O_4 from industrial Cu sludge with irregular surface morphology via combustion route [17]. Furthermore, irregular surface morphology with low value of saturation magnetization (7.24 emu g^{-1}) nanodimension CuFe_2O_4 has been synthesized by Hankare et al. by autocombustion sol–gel process [18]. Wang et al. have prepared irregular mesoporous CuFe_2O_4 with low value of saturation magnetization [19]. Nanocrystallite CuFe_2O_4 has been prepared by Khedr et al. via flash combustion method [20]. There are impurities also obtained with the desired phase. Synthesis of irregular surface morphology of CuFe_2O_4 with impurities ($\alpha\text{-Fe}_2\text{O}_3$) via decomposition process has been reported by Randhawa et al. [21]. Selvan et al. reported synthesis of CuFe_2O_4 by combustion process [22]. However, $\alpha\text{-Fe}_2\text{O}_3$ is obtained as an impurity. We are trying to synthesize nanocrystallite CuFe_2O_4 via simple complexometric method with proper surface morphology.

Catalytic applicability is another important area for these spinel group materials as compared to common iron hydroxides (Fe_3O_4 , $\alpha\text{-Fe}_2\text{O}_3$, and $\alpha\text{-FeOOH}$). Many of them have been shown to be effective for dye degradation due to their stable structure, low band gap energy, and excellent magnetic properties [23]. The low efficiency of converting solar energy into chemical energy greatly restricts their applications in photocatalytic reaction. Recent study exhibits that CuFe_2O_4 has been widely used as a heterogeneous photosensitive Fenton catalyst due to its narrow band gap [24–26], excellent visible-light response, low cost, and good photochemical stability. Sharma et al. [27] has been reported that CuFe_2O_4 acts as a better catalyst as compared to CoFe_2O_4 , NiFe_2O_4 , and ZnFe_2O_4 in the optimum reaction conditions, which may be attributed to coupling between $\text{Fe}^{2+}/\text{Fe}^{3+}$ and $\text{Cu}^+/\text{Cu}^{2+}$ redox pairs, thus generating more efficient Fenton reagent under illumination. Furthermore, the photocatalytic activity of CuFe_2O_4 in photo-Fenton-type reaction [23, 28, 29] has been affected by rapid recombination of electron-hole pairs, a high value of ion leaching, and a low ratio of surface area to mass. Several attempts had been introduced to reduce the recombination of photoinduced electron-hole pairs and increase the photocatalytic efficiency of material by synthesizing various structures, doping with other elements, coupling with other semiconductors, and supporting with other materials. Till date, methylene blue (MB) degradation by hydrogen peroxide has been reported with systems that employ classical Fenton oxidation with various transition metal ferrites [30–34], silica-titania supported ferrites [35, 36] or ferrite material bound to

polymeric support complex [37]. A significant issue is the separation of catalyst from the reaction medium. In many cases, this is unfeasible due to technical and/or economical constraints. The use of homogeneous transition metal ion complex as catalysts is not effective due to their toxic and harmful nature as well as their difficult separation process for repeated use. It is thus highly desirable to synthesize heterogeneous magnetic CuFe_2O_4 as catalyst for this purpose.

With this perspective, we report in the present work a simple procedure to synthesis of copper ferrite with narrow size distribution by a single-step modified complexometric process. In this process, we have used EDTA as the complexing agent and CA as the fuel. We have explored the material properties (micro-structure, optical and magnetic) as well as photocatalytic behavior (for MB degradation) of this ferrite material. This facile synthetic approach is projected to be an effective, low-cost fabrication process that has a high potential for scaling up.

Experimental

All chemicals were of analytical grade and used as purchased without further purification. The precursors used are nitrate salts of copper(II) and iron(III) procured from E-Merck, India. The purity levels of all precursors are at $>99.9\%$. EDTA and CA are purchased from Merck, India ($>99.9\%$). Oxidant 30% H_2O_2 from Merck, India and dye methylene blue (82%) from Loba Chemie, India were used.

In a typical synthesis, the stoichiometric amounts of Cu(II)–nitrate (0.001 mol) and Fe(III)–nitrate (0.002 mol) were dissolved in minimum amount of deionized water under stirring condition at room temperature. The resulting solution was stirred for about 30 min to make it homogeneous. The measured amount of EDTA (0.002 mol) was then added into the metal nitrate solution. Subsequently, calculated amount of CA (0.002 mol) was added in the reaction mixture at stirring condition. After this addition, the total mixture was stirred for 1 h to make it homogeneous. Then, the solution was burned in spot furnace at 300°C . After complete combustion, a blackish red powder was produced. This precursor was calcined at various temperatures (based on TGA-DSC studies as detailed below) to obtain the desired ferrite material.

Thermal gravimetric analysis (TGA) and differential scanning calorimetric (DSC) studies were performed using Diamond Pyris 480, PerkinElmer instrument under nitrogen flow of 150 mL min^{-1} with a heating rate of $15^\circ\text{C min}^{-1}$ using $\alpha\text{-Al}_2\text{O}_3$ as the standard to study the changes due to thermal effect at predetermined programmed rate. Powder X-ray diffraction data were collected in a Bruker D8 advance X-ray diffractometer using Lynxeye detector (1 D mode). The patterns were run with $\text{Cu K}\alpha = 1.5418 \text{ \AA}$ at 40 kV and 40 mA with step size of 0.02° . The textural properties of the catalysts

were investigated by the N_2 sorption analysis. The N_2 sorption isotherm was measured at $-195\text{ }^\circ\text{C}$ using NovaWin2 (Quantachrome instruments, USA). Before each measurement, the sample was degassed at $110\text{ }^\circ\text{C}$ for about 3 h. The optical behavior was analyzed by UV–Vis spectroscopy (PerkinElmer, Lambda 35) in the range of 200 to 800 nm in absorption mode. Molecular signature of the sample was determined by FT-IR (model Prestige 21, Shimadzu) in transmittance mode in the range of 400 to 4000 cm^{-1} . Two milligrams of solid sample was mixed with 200 mg of vacuum-dried IR-grade KBr. The mixture was dispersed by grinding for 3 min in a vibratory ball mill and placed in a steel die of 10 mm diameter and subjected to a pressure of 12 t. The sample disk was placed in the holder of the double grating IR spectrometer. The morphological behavior of the material was recorded on a scanning electron micrograph (SEM, model JAX-840A, JEOL) and field emission scanning electron microscopy (FE-SEM, model S-4800, Hitachi). The composition analysis of the material was carried out by EDX using INC X Oxford under the acceleration voltage set at 10 keV. High-resolution transmission electron microscopy (HR-TEM) study was carried in JEOL-JEM-2100. The sample was dispersed in ethanol and then treated ultrasonically in order to disperse individual particles over carbon coated copper grids for analysis. Surface topological study was recorded by atomic force micrographs (AFM) on nano-K vibration isolation by minus-K technology (NTMDT) in semiconductive method. Magnetic measurement was carried out at room temperature using vibrating sample magnetometer (VSM, Lake Shore 7407 series) with a maximum magnetic field of 20 kOe.

Results and discussion

Figure 1 shows the TGA-DSC curves of the copper ferrite precursor. In the diagram, the red line indicates the nature of heat flow during heat treatment and the green line denotes the weight change with respect to the programmed temperature. The endothermic peak at around $100\text{ }^\circ\text{C}$ occurs due to the remove of volatile material and water molecule. The exothermic peak at $\sim 520\text{ }^\circ\text{C}$ may be attributed to the decomposition of metal-EDTA complex into their corresponding metal oxides. During the heat treatment, the mass change of the precursor takes place in two definite steps. The major weight loss of $\sim 53\%$ up to $400\text{ }^\circ\text{C}$ is due to the removal of volatile material (ethylene glycol and water). Beyond this temperature $\sim 30\%$, mass of the ferrite precursor is reduced due to the decomposition of metal-EDTA complex. The plateau formed beyond $800\text{ }^\circ\text{C}$ suggests the formation of a stable ferrite phase. From the TGA-DSC studies, we thus chose three calcination temperatures, namely 400 , 600 , and $800\text{ }^\circ\text{C}$, and the heating rate of $5\text{ }^\circ\text{C min}^{-1}$ for 4 h to obtain the desired ferrite materials, named respectively as CuFe4, CuFe6, and CuFe8.

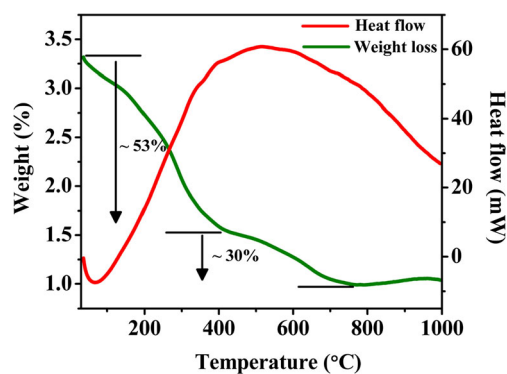


Fig. 1 TGA-DSC curves of the copper ferrite precursor

Figure 2 shows the X-ray diffraction patterns of the copper ferrite materials obtained on calcination at various temperatures. The diffraction peaks have been indexed to (101), (112), (200), (103), (211), (202), (004), (220), (312), (105), (303), (321), (224), (400), (413), and (404) reflection planes of the tetragonal body center cubic lattice of CuFe_2O_4 (JCPDS PDF # 34-0425). This confirms formation of single phase copper ferrite in the synthesis procedure. There are some impurities observed along with the desire ferrite at low calcination temperature (400 and $600\text{ }^\circ\text{C}$). As expected, the sharpness and intensity of the diffraction peaks of copper ferrite increase with the increase in calcination temperature. This is due to enhancement of crystallinity of the nanoparticles. Owing to its best phase characteristics, we have chosen the sample obtained on calcination at $800\text{ }^\circ\text{C}$ (CuFe8) for most of the subsequent studies.

The crystallite size of the materials has been calculated by using the Scherrer's Eq. (1):

$$D = \frac{0.9\lambda}{\beta \cos\theta} \quad (1)$$

where D is the average crystallite size of the phase under investigation, λ is the wavelength of X-ray, β is the full width at half maximum (FWHM) of the diffraction peak, and θ is the Bragg angle. The crystallite sizes of CuFe_2O_4 are found in the range 13–30 nm depending on the calcination temperature.

The BET-specific surface area and pore volume of CuFe8 are measured to be $32\text{ m}^2\text{ g}^{-1}$ and 0.14 g cm^{-3} , respectively. The pore diameter of this material is found to be below 21 nm. It confirms that CuFe8 behaves as a mesoporous material (diameter of the mesopore being 2–50 nm). This observation suggests that the specific surface areas of the CuFe_2O_4 material are improved compared with some of the literature reports [38–40]. Faungnawakij and coworkers synthesized CuFe_2O_4 as a catalyst for steam reforming by complexometric method using CA as a complexing agent with BET surface area ($1\text{ m}^2\text{ g}^{-1}$) [38]. Nanodimension CuFe_2O_4 has been synthesized via microwave-induced combustion process by Liu et al. with specific surface area ($6\text{ m}^2\text{ g}^{-1}$) [39]. Anandan et al.

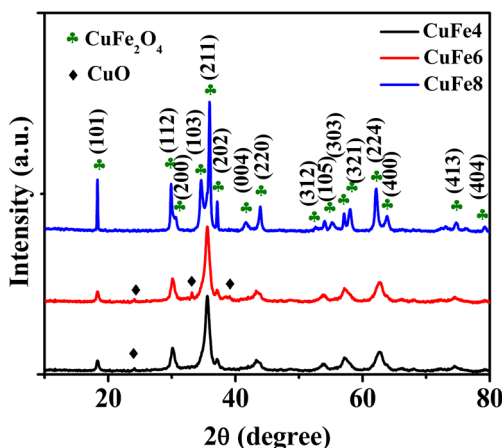


Fig. 2 XRD patterns of copper ferrites precursors at various calcined temperature

reported synthesis of irregular surface morphology CuFe_2O_4 with BET surface area ($14 \text{ m}^2 \text{ g}^{-1}$) [40].

Figure 3 shows the absorption spectrum of the finalized ferrite material. The absorption behavior of the ferrite material is originated due to the charge transfer between the metal ions. Haart and his coworkers have proposed that the metal to metal charge transfer transition takes place in two ways. The charge transfer transition takes places between Fe^{3+} and Fe^{2+} in the ferrite system, and the other absorptions may be due to the electron transfer in between O(2p) level and the Fe(3d) level.

The direct band gap value of the material is measured by using the Tauc's equation (Eq. (2)):

$$(\alpha h\nu)^2 = A(h\nu - E_g) \quad (2)$$

where $h\nu$ is the photon energy, E_g denotes the band gap value, α is the absorption coefficient, and A is a constant. The absorption coefficient α may be expressed as follows:

$$\alpha = 2.303 \left(\frac{A_b}{t} \right) \quad (3)$$

In the above equation, A_b is the absorbance and t is the thickness of cuvette. Figure 3 also depicts the $(\alpha h\nu)^2$ vs. $h\nu$ curves, from which the band gap of CuFe8 determined by the method of extrapolation to be 1.40 eV.

Figure 4 represents the FT-IR spectrum of CuFe8. The spinel ferrites exhibit two main adsorption bands below 1000 cm^{-1} , due to the presence of metal–oxygen vibration mode. In the ferrite system, the metal ions are distributed among the two sublattices, namely tetrahedral (A sites) and octahedral (B sites). The bands centered at 400 cm^{-1} and 600 cm^{-1} are attributed to the stretching mode of the octahedral complex (ν_2) and tetrahedral complex (ν_1), respectively [41]. The peak at $\sim 572 \text{ cm}^{-1}$ is ascribed to stretching vibration of the tetrahedral sites, and the band at $\sim 420 \text{ cm}^{-1}$ is due to the octahedral sites in spinel compounds [42]. The band at 1037 cm^{-1} may be contributed to the Fe–Cu stretching. The

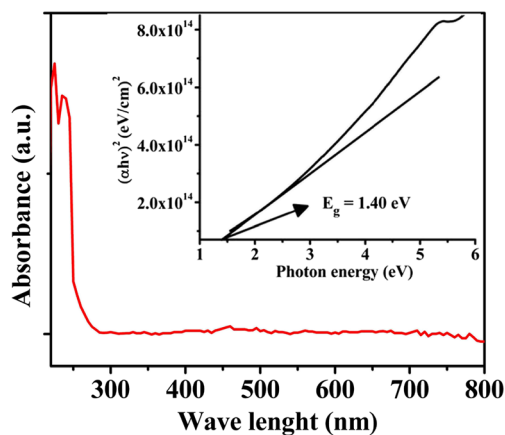


Fig. 3 UV–Vis spectrum and plot of $(\alpha h\nu)^2$ vs. photoenergy (eV) of CuFe8

broad absorption band at $\sim 3432 \text{ cm}^{-1}$ is attributed to the stretching of OH. The band at around 1421 cm^{-1} may be attributed to the symmetrical stretching vibrations of CO_2 .

Figure 5a–d depicts the SEM images of CuFe8 at various resolutions. The material is porous in nature. The pores are generated due to the evolved gases during the heat treatment process. The grain boundary separation between two neighboring particle is easily isolable. The particles are agglomerated in nature. However, for better understanding of the surface morphology, we carried out FE-SEM and AFM studies. The agglomeration of the particle is related to various factors such as shape, surface area, and energy or magnetic interaction among them. Such kind of agglomeration also enhances the mechanical properties of material (hardness, density, and ductility).

Figure 5e shows representative EDX spectrum of CuFe8. The EDX spectra indicate the presence of Cu, Fe, and O as constituent elements in the ferrite materials. The relative atomic abundance and weight percentage of the elements present are included in the spectra also (see Fig. 5e). The atomic ratio of Cu/Fe is found to be 0.45 that is lower than the theoretically

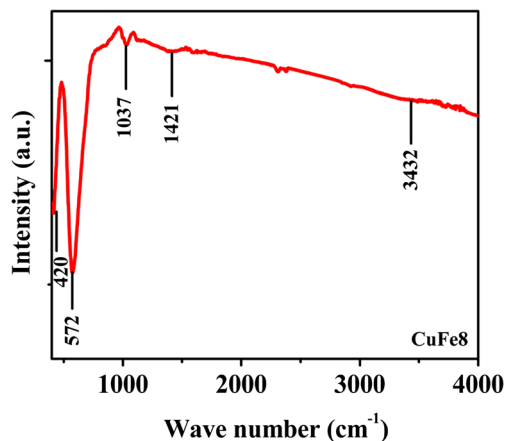


Fig. 4 FT-IR spectrum of CuFe8

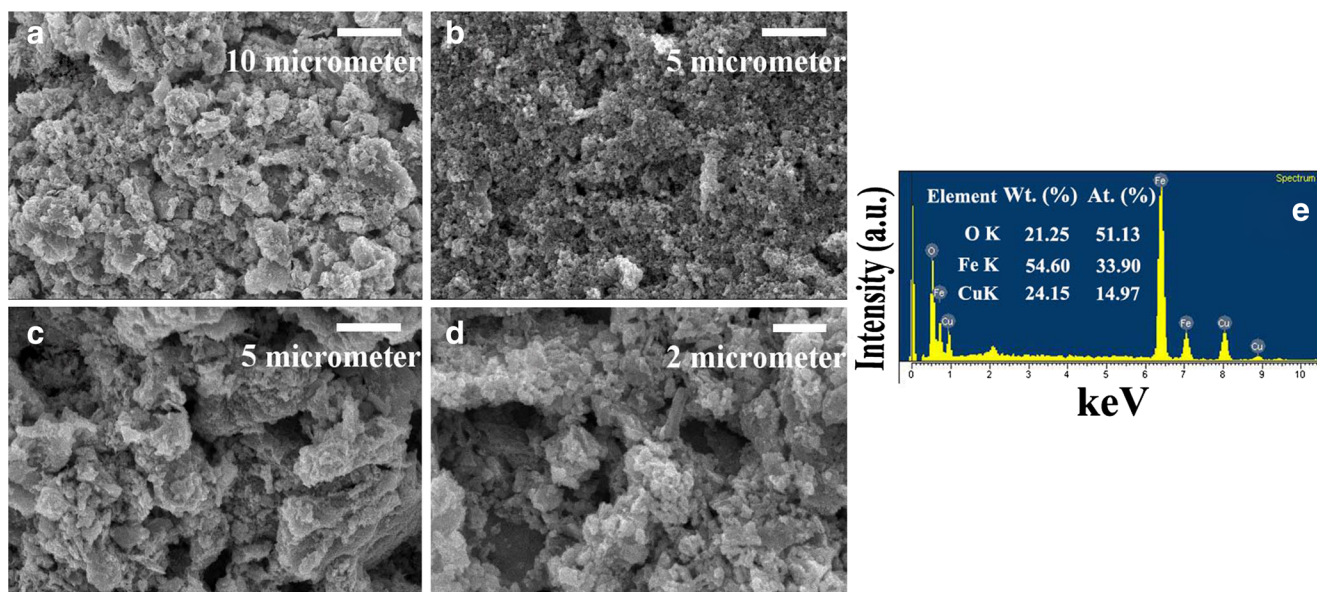


Fig. 5 a–d SEM and e EDX images of CuFe₈, respectively

expected value. Such kind of deviation may be caused by the structural defects present in the sample.

Figure 6 shows the FE-SEM images of CuFe₈. The surface morphology of CuFe₈ is almost spherical in nature. The grain boundary between two neighboring particle is connected. There are some pores observed in the synthesized ferrite material (see Fig. 6a, d). The particle size of the CuFe₈ is measured to be around 25 nm.

Figure 7a, b represents the general view of CuFe₈ whereas HR-TEM image of an isolated particle is included in Fig. 7c. The particles are spherical in shape with average size ~ 32 nm as evidenced in the FE-SEM studies. Moreover, the HR-TEM image for CuFe₈ displays distinct lattice spacing of 2.52 Å corresponding to (211) planes (see Fig. 7c).

The selected area electron diffraction (SAED) patterns (see Fig. 7d) of the CuFe₈ exhibit ring type diffraction pattern revealing their polycrystalline nature. The rings indicated in the figure correspond to the diffraction planes (202), (211), and (103) for CuFe₈.

Figure 8 shows the surface topographic view of CuFe₈. The spherical copper ferrite particles are homogeneously distributed throughout the surface (see Fig. 8). The material exhibits equal size distribution. The surface topographic view of the ferrite material looks like a semisphere.

Figure 9 depicts the M–H curves of CuFe₈ at room temperature. The magnetic properties such as saturation magnetization (M_s), remanence magnetization (M_r), coercivity (H_c), and magnetic moment (η_B) of the material are measured. The magnetic properties of the ferrite materials are significantly changed compared to their bulk state. The crystallite size influences the magnetic behavior of material in nanodimension regime [43]. The M_s and M_r values of CuFe₈ are measured to be 52.40 and 40.30 emu g⁻¹, respectively. From the hysteresis

loops, the loop squareness ratio ($R = 0.77$) of the remnant to the saturation magnetization (M_r/M_s) is calculated to determine the inter- and intra-grain exchange interactions, sublattice magnetization, magnetic anisotropy, and morphology of the sample [44, 45]. However, the H_c value is determined to be 148.90 Oe. From the nature of the curve, it may be concluded that the sample acts as a soft type magnetic material.

It is observed that the magnetic behavior of copper ferrite is enhanced compared with some of the literature reports. Table 1 compares the magnetic properties of various literature reports (most relevant ones) of copper ferrite material with our work.

CuFe₂O₄ has a unique property, namely it exists in both the tetragonal and the cubic phases. However, at higher calcination temperature, tetragonal phase is more stable than the cubic phase [52]. CuFe₂O₄ has inverse spinel structure in the tetragonal phase. In this case, the octahedral sublattices are occupied by all the Cu²⁺ ions, whereas Fe³⁺ ions divide equally between the tetrahedral and octahedral sublattices [53]. The cubic phase contributes more magnetic moment than the tetragonal phase. It is due to the presence of more number of cupric ions (Cu²⁺) at the tetrahedral sites of the cubic phase in comparison to the tetragonal phase.

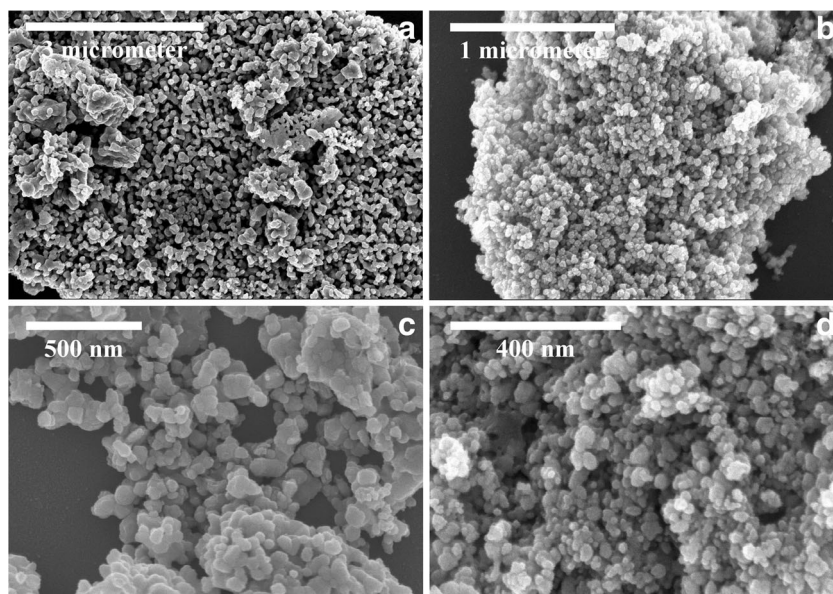
The magnetic moment (η_B) in Bohr magneton is calculated using the following formula:

$$\eta_B = M_w \times M_s / 5585 \quad (4)$$

where M_w represents the molecular weight (in g), and M_s denotes the saturation magnetization (emu g⁻¹) of the substance. The unit of η_B is emu.

The degradation of MB is carried out in the absence as well as in presence of the CuFe₈ due to the better crystallinity as

Fig. 6 FE-SEM images of CuFe₈ under different resolutions



well as phase purity. The reaction conditions have been decided on the basis of our previous study for MB degradation study [34]. The pH of the medium plays a crucial role in dye degradation, and hence, we have explored the effect of different pH, acidic (pH = 4), neutral (pH = 7), and alkaline (pH = 9).

The photocatalytic activity of MB degradation is measured by applying the following equation:

$$\text{Degradation}(\%) = \left[\frac{C_0 - C}{C_0} \right] \times 100 \quad (5)$$

where C_0 is the initial concentration of MB, and C is the concentration of MB after degradation for certain time. The

C_0/C ratio can be replaced by A_0/A because the concentration (C) is directly proportion to the absorbance (A).

Figure 10 exhibits the MB degradation patterns at different pH over CuFe₈. In the absence of catalyst, only 7% degradation takes place after 3 h. The intensity of blue colored mixture gradually vanished with the progress of the time that indicated the degradation of MB that occurred with different rates in different pH media. The CuFe₈ shows the best photocatalytic activity in acidic medium compared to neutral and basic medium. About 96% MB is degraded after 45 min over CuFe₈ in acidic medium, whereas these values are 92 and 60% after 60 min at pH = 7 and pH = 9, respectively. The low band gap value and high surface energy enhance the photocatalytic activity of the material.

Fu and coworkers have studied MB degradation over CuFe₂O₄-graphene composite material in the presence of UV radiation. It degraded ~96% of MB within 240 min [46]. Albuquerque et al. have found that CuFe₂O₄ degrades ~35% of MB after 150 min under the same reaction condition [54]. Guo et al. has carried out MB degradation over graphite carbon coating CuFe₂O₄ in the presence of light irradiation and H₂O₂ as oxidizing agent [55]. It is found that ~97% of MB is degraded over this catalyst in 80 min. Anandan and coworkers explored MB degradation over different kinds of oxidant under the presence of UV light [40]. It has been reported that only 16% of dye is degraded over CuFe₂O₄ in 75 min. However, 95% of MB is degraded in the presence of oxidant (peroxydisulfate) over same catalyst (in same time interval). Zhuang et al. carried out degradation of MB in the presence of reducing agent NaBH₄ over CuFe₂O₄ [56]. It takes 8 min for almost 100% degradation. However a negligible amount of dye degrades in 50 min over only CuFe₂O₄. From this study, it may be concluded that synthesized material shows better

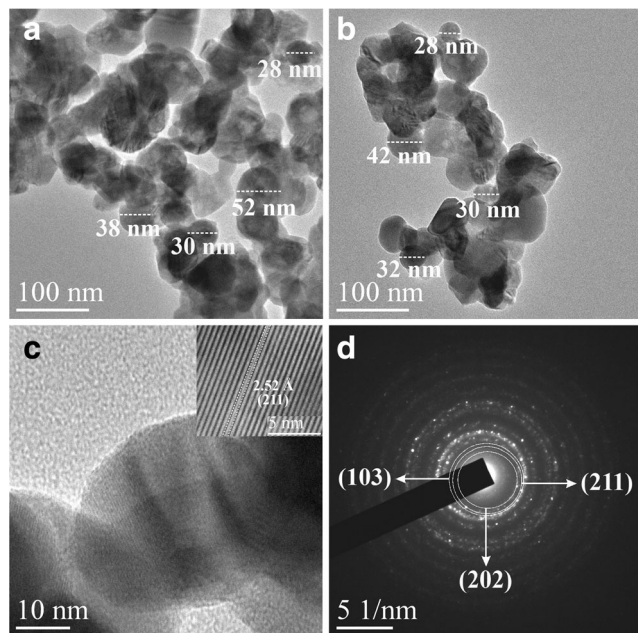


Fig. 7 a–c HR-TEM image and d SAED pattern of CuFe₈

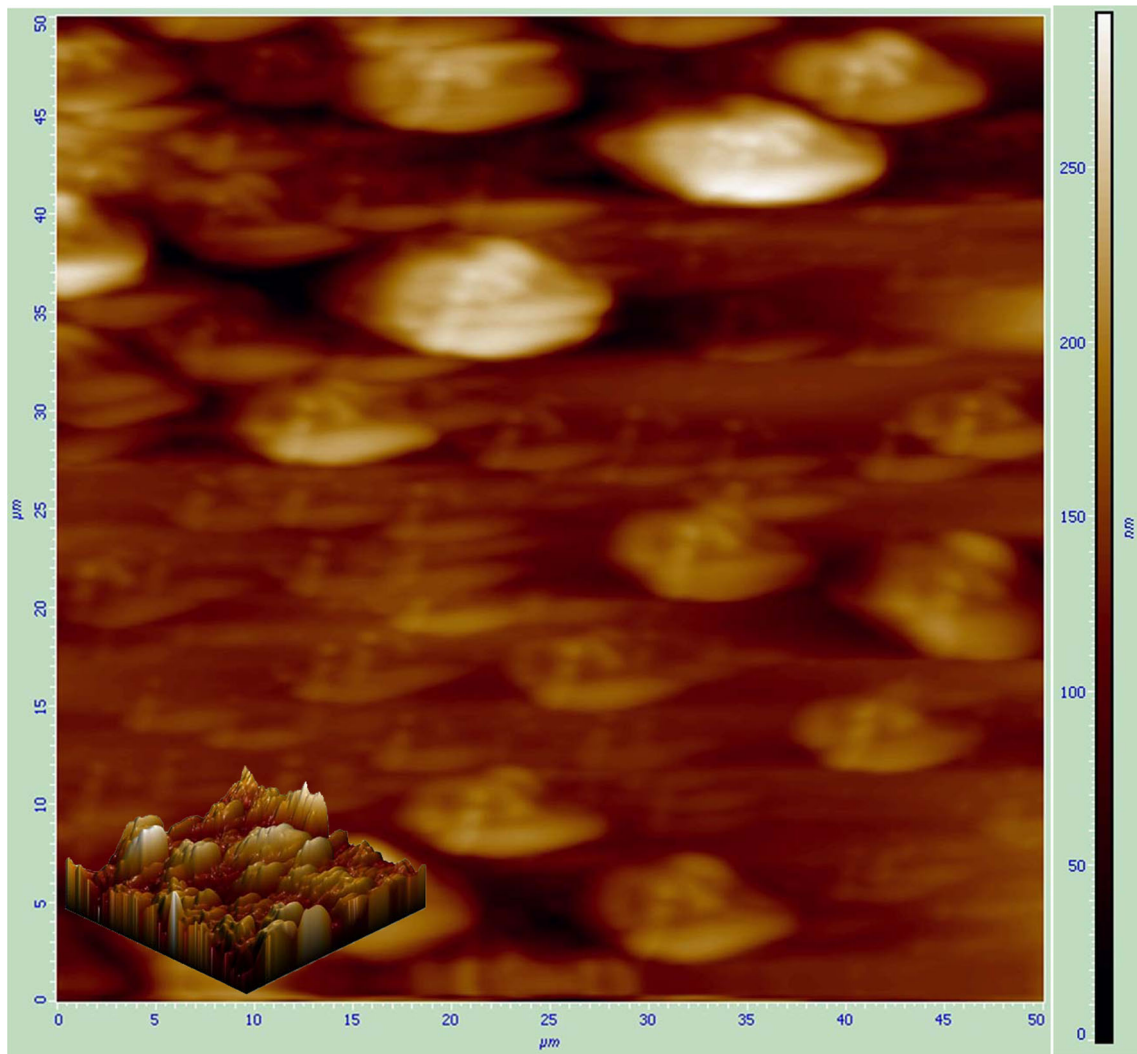


Fig. 8 AFM image of CuFe8

photocatalytic activity compared with some of the previous literature reports.

The photocatalytic degradation of MB follows a first-order kinetic reaction (Eq. (6)):

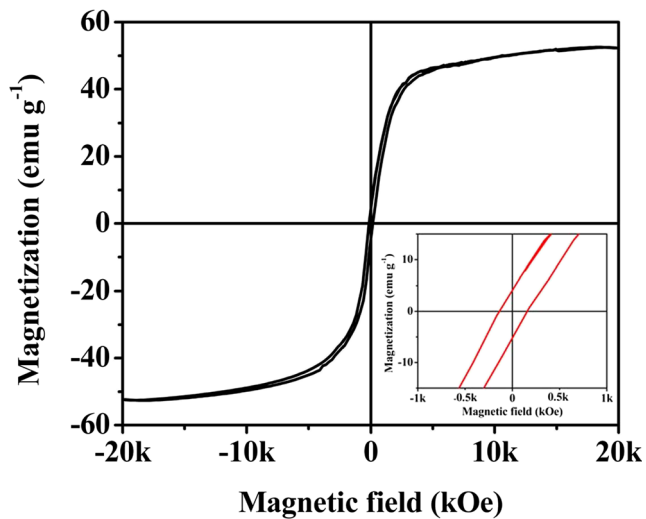


Fig. 9 M-H curve of CuFe8 at room temperature

Table 1 Comparison of magnetic properties of CuFe₂O₄

Material	M_s (emu g ⁻¹)	M_r (emu g ⁻¹)	M_r/M_s	Hc (Oe)	Reference
CuFe ₂ O ₄	7.23	3.65	0.50	1576.6	[18]
	27.59	4.40	0.16	288.45	[19]
	48.05	9.30	0.19	76.00	[43]
	22.21	6.70	0.30	1704.41	[46]
	40.03	36.53	0.91	779.54	[47]
	19.00	–	–	–	[48]
	8.90	1.89	0.21	225.3	[49]
	37.38	0.81	0.02	26.38	[50]
	1.36	0.52	0.38	444.90	[51]
	52.40	40.30	0.77	148.90	This work

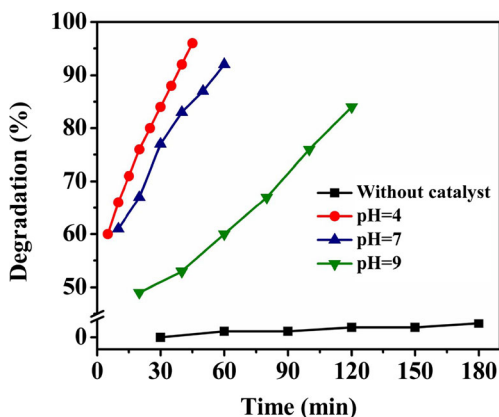


Fig. 10 Degradation behavior of MB over CuFe8 at pH = 4 (filled circle), pH = 7 (filled triangle), and pH = 9 (filled inverted triangle)

$$\ln\left(\frac{C_0}{C}\right) = kt \quad (6)$$

where k is the rate constant, and t is the reaction time. The plots of $\ln(C_0/C)$ vs. time give a straight line (see Fig. 11) indicating first-order reaction for the photocatalytic degradation. The slopes yield apparent rate constants (k) of degradation. The magnitude of k is highest in the acidic medium compared to the neutral or alkaline medium. Particularly, the magnitude of k is 5.24×10^{-2} and $1.14 \times 10^{-2} \text{ min}^{-1}$, respectively, in the acidic and basic media. For neutral medium, the value is $3.14 \times 10^{-2} \text{ min}^{-1}$. The present findings thus project this modified complexometric process as a fascinating method to synthesize nanostructured ferrite material with good photodegradation behavior under visible light in the presence of peroxide oxidant.

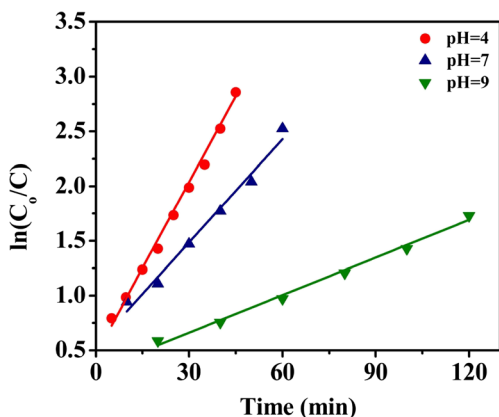


Fig. 11 $\ln(C_0/C)$ vs. time plot at pH = 4 (filled circle), pH = 7 (filled triangle), and pH = 9 (filled inverted triangle) for MB degradation over CuFe8

Conclusions

Nanostructured polycrystalline copper ferrite has been successfully synthesized by a modified complexometric method using EDTA as a complexing agent and citric acid as a fuel, respectively. The crystallite size of copper ferrite is found in the region 13–30 nm depending on the calcination temperature. The surface morphology of the material is spherical. The particles are almost equal in size and homogeneously distributed throughout the surface. The BET-specific surface area and the pore diameter of the CuFe8 are $32 \text{ m}^2 \text{ g}^{-1}$ and 21 nm, respectively. It confirms that CuFe8 behaves as a mesoporous material. Copper ferrite has an agglomeration tendency due to magnetic interaction among the particle and high surface energy. The ferrite material shows significant photocatalytic degradation of MB under the visible light in the presence of H_2O_2 . In particular, it degrades 96% of MB in acidic medium (pH = 4) after 45 min. The synthetic procedure is simple, facile, economical, and ecofriendly.

Acknowledgements One of the authors (MS) is thankful to UGC for a fellowship. The authors would like to thank Department of Metallurgical & Material Engineering, Department of Chemistry, and School of Material Science & Nanotechnology, Jadavpur University for providing the instrumental facilities.

Funding information Financial support from the Department of Science and Technology, Government of India, by a grant (EMR/2016/001811) to AG is gratefully acknowledged.

References

- Polshettiwar, V., Luque, R., Fihri, A., Zhu, H.B., Bouhrara, M., Basset, J.M.: Magnetically Recoverable Nanocatalysts. *Chem Rev.* **111**, 3036–3075 (2011)
- Sartale, S.D., Lokhande, C.D., Muller, M.: Electrochemical synthesis of nanocrystalline CuFe2O4 thin films from non-aqueous (ethylene glycol) medium. *Mater Chem Phys.* **80**, 120–128 (2003)
- Sun, Z., Liu, L., Jia, D.Z., Pan, W.: Simple synthesis of CuFe2O4 nanoparticles as gas-sensing materials. *Sens Actuators B: Chem.* **125**, 144–148 (2007)
- Kang, K.S., Kim, C.H., Cho, W.C., Bae, K.K., Woo, S.W., Park, C.S.: Reduction characteristics of CuFe2O4 and Fe3O4 by methane; CuFe2O4 as an oxidant for two-step thermochemical methane reforming. *Int J Hydrogen Energy.* **33**, 4560–4568 (2008)
- Kameoka, S., Tanabe, T., Tsai, A.P.: Self-assembled porous nanocomposite with high catalytic performance by reduction of tetragonal spinel CuFe2O4. *Appl Catal A: G E N.* **375**, 163–171 (2010)
- Nasrallah, N., Kebir, M., Koudri, Z., Trari, M.: Photocatalytic reduction of Cr(VI) on the novel hetero-system CuFe2O4/CdS. *J Hazard Mater.* **185**, 1398–1404 (2011)
- Selvan, R.K., Kalaiselvi, N., Augustin, C.O., Doh, C.H., Sanjeeviraja, C.: CuFe2O4/SnO2 nanocomposites as anodes for Li-ion batteries. *J Power Sources.* **157**, 522–527 (2006)
- Roy, S., Ghose, J.: Mössbauer study of nanocrystalline cubic CuFe2O4 synthesized by precipitation in polymer matrix. *J Magn Magn Mater.* **307**, 32–37 (2006)
- Sugimoto, M.: The past, present, and future of ferrites. *J Am Ceram Soc.* **82**, 269–280 (1999)

10. Tasca, J.E., Quincoces, C.E., Lavat, A., Alvarez, A.M., González, M.G.: Preparation and characterization of CuFe₂O₄ bulk catalysts. *Ceram Int*. **37**, 803–812 (2011)
11. Tsoncheva, T., Manova, E., Velinov, N., Paneva, D., Popova, M., Kunev, B., Tenchev, K., Mitov, I.: Thermally synthesized nanosized copper ferrites as catalysts for environment protection. *Catal Commun*. **12**, 105–109 (2010)
12. Liu, T., Wang, L., Yang, P., Hu, B.: Preparation of nanometer CuFe₂O₄ by auto-combustion and its catalytic activity on the thermal decomposition of ammonium perchlorate. *Mater Lett*. **62**, 4056–4058 (2008)
13. Altincekic, T.G., Boz, I., Baykal, A., Kazan, S., Topkaya, R., Toprak, M.S.: Synthesis and characterization of CuFe₂O₄ nanorods synthesized by polyol route. *J Alloys Compd*. **493**, 493–498 (2010)
14. Du, J., Liu, Z., Wu, W., Li, Z., Han, B., Huang, Y.: Preparation of single-crystal copper ferrite nanorods and nanodisks. *Mater Res Bull*. **40**, 928–935 (2005)
15. Ponhan, W., Maensiri, S.: Fabrication and magnetic properties of electrospun copper ferrite CuFe₂O₄ nanofibers. *Solid State Sci*. **11**, 479–484 (2009)
16. Yan, K., Wu, X., An, X., Xie, X.: Facile synthesis and catalytic property of spinel ferrites by a template method. *J Alloys Compd*. **552**, 405–408 (2013)
17. Tu, Y.J., Chang, C.K., You, C.F.: Combustion of isopropyl alcohol using a green manufactured CuFe₂O₄. *J Hazard Mater*. **229–230**, 258–264 (2012)
18. Hankare, P.P., Sanadi, K.R., Pandav, R.S., Patil, N.M., Garadkar, K.M., Mulla, I.S.: Structural, electrical and magnetic properties of cadmium substituted copper ferrite by sol–gel method. *J Alloys Compd*. **540**, 290–296 (2012)
19. Wang, Y., Zhao, H., Li, M., Fan, J., Zhao, G.: Magnetic ordered mesoporous copper ferrite as a heterogeneous Fenton catalyst for the degradation of imidacloprid. *Appl Catal B Environ*. **147**, 534–545 (2014)
20. Khedry, M.H., Farghali, A.A.: Physicochemical properties of nanocrystallite copper ferrite prepared by a novel self flash combustion of acetate precursors. *J Mater Sci Technol*. **21**, 675–680 (2005)
21. Randhawa, B.S., Dosanjh, H.S., Kaur, M.: Preparation of spinel ferrites from citrate precursor route—A comparative study. *Ceram Int*. **35**, 1045–1049 (2009)
22. Selvan, R.K., Augustin, C.O., Berchmans, L.J., Saraswathi, R.: Combustion synthesis of CuFe₂O₄. *Mater Res Bull*. **38**, 41–54 (2003)
23. Wang, Y.B., Zhao, H.Y., Li, M.F., Fan, J.Q., Zhao, G.H.: Magnetic ordered mesoporous copper ferrite as a heterogeneous Fenton catalyst for the degradation of imidacloprid. *Appl Catal B*. **147**, 534–545 (2014)
24. Yao, Y.J., Lu, F., Zhu, Y.P., Wei, F.Y., Liu, X.T., Lian, C., Wang, S.B.: Magnetic core–shell CuFe₂O₄@C₃N₄ hybrids for visible light photocatalysis of Orange II. *J Hazard Mater*. **297**, 224–233 (2015)
25. Cheng, R.L., Fan, X.Q., Wang, M., Li, M.L., Tian, J.J., Zhang, L.X.: Facile construction of CuFe₂O₄/g-C₃N₄ photocatalyst for enhanced visible-light hydrogen evolution. *RSC Adv*. **6**, 18990–18995 (2016)
26. Zhao, W., Jin, Y., Gao, C.H., Gu, W., Jin, Z.M., Lei, Y.L., Liao, L.S.: A simple method for fabricating p–n junction photocatalyst CuFe₂O₄/Bi₄Ti₃O₁₂ and its photocatalytic activity. *Mater Chem Phys*. **143**, 952–962 (2014)
27. Sharma, R., Singhal, S.: Photodegradation of textile dye using magnetically recyclable heterogeneous spinel ferrites. *J Chem Technol Biotechnol*. **90**, 955–962 (2015)
28. Ding, Y.B., Zhu, L.H., Wang, N., Tang, H.Q.: Sulfate radicals induced degradation of tetrabromobisphenol A with nanoscaled magnetic CuFe₂O₄ as a heterogeneous catalyst of peroxymonosulfate. *Appl Catal B*. **129**, 153–162 (2013)
29. Zhang, T., Zhu, H.B., Croué, J.P.: Production of Sulfate Radical from Peroxymonosulfate Induced by a Magnetically Separable CuFe₂O₄ Spinel in Water: Efficiency, Stability, and Mechanism. *Environ Sci Technol*. **47**, 2784–2791 (2013)
30. Jauhar, S., Singhal, S., Dhiman, M.: Manganese substituted cobalt ferrites as efficient catalysts for H₂O₂ assisted degradation of cationic and anionic dyes: Their synthesis and characterization. *Appl Catal A*. **486**, 210–218 (2014)
31. Sharma, R., Bansalb, S., Singhal, S.: Tailoring the photo-Fenton activity of spinel ferrites (MFe₂O₄) by incorporating different cations (M = Cu, Zn, Ni and Co) in the structure. *RSC Adv*. **5**, 6006–6018 (2015)
32. Senapatia, K.K., Borgohain, C., Sarma, K.C., Phukan, P.: Photocatalytic degradation of methylene blue in water using CoFe₂O₄–Cr₂O₃–SiO₂ fluorescent magnetic nanocomposite. *J Mol Catal A Chem*. **346**, 111–116 (2011)
33. Jia, Z., Ren, D., Liang, Y., Zhu, R.: A new strategy for the preparation of porous zinc ferrite nanorods with subsequently light-driven photocatalytic activity. *Mater Lett*. **65**, 3116–3119 (2011)
34. Saha, M., Mukherjee, S., Kumar, S., Dey, S., Gayen, A.: Albumin matrix assisted wet chemical synthesis of nanocrystalline MFe₂O₄ (M = Cu, Co and Zn) ferrites for visible light driven degradation of methylene blue by hydrogen peroxide. *RSC Adv*. **6**, 58125–58136 (2016)
35. Zhang, G.Y., Sun, Y.Q., Gao, D.Z., Xu, Y.Y.: Quasi-cube ZnFe₂O₄ nanocrystals: Hydrothermal synthesis and photocatalytic activity with TiO₂ (Degussa P25) as nanocomposite. *Mater Res Bull*. **45**, 755–760 (2010)
36. Li, Y., Dong, X., Li, J.: Synthesis and characterization of super paramagnetic composite photocatalyst–Titania/silica/nickel ferrite. *Particulogy*. **9**, 475–479 (2011)
37. Ma, S.D., Feng, J., Qin, W.J., Juab, Y.Y., Chen, X.G.: CuFe₂O₄@PDA magnetic nanomaterials with a core–shell structure: synthesis and catalytic application in the degradation of methylene blue in water. *RSC Adv*. **5**, 53514–53523 (2015)
38. Faungnawakij, K., Tanaka, Y., Shimoda, N., Fukunaga, T., Kikuchi, R., Eguchi, K.: Hydrogen production from dimethyl ether steam reforming over composite catalysts of copper ferrite spinel and alumina. *Appl Catal B*. **74**, 144–151 (2007)
39. Liu, Y.C., Fu, Y.P.: Magnetic and Catalytic properties of copper ferrite nanopowders prepared by a microwave induced combustion process. *Ceram Int*. **36**, 1597–1601 (2010)
40. Anandan, S., Selvamani, T., Prasad, G.G., Asiri, A.M., Wu, J.J.: Magnetic and catalytic properties of inverse spinel CuFe₂O₄ nanoparticles. *J Magn Magn Mater*. **432**, 437–443 (2017)
41. Waldron, R.D.: Infrared Spectra of Ferrites. *Phys Rev*. **99**, 1727–1735 (1955)
42. Banerjee, A.M., Pai, M.R., Meena, S.S., Tripathi, A.K., Bharadwaj, S.R.: Catalytic activities of cobalt, nickel and copper ferrosinels for sulfuric acid decomposition: The high temperature step in the sulfur based thermochemical water splitting cycles. *Int J Hydrogen Energy*. **36**, 4768–4780 (2011)
43. Deraz, N.M.: Size and crystallinity-dependent magnetic properties of copper ferrite nano-particles. *J Alloys Compd*. **501**, 317–325 (2010)
44. Caizer, C., Stefanescu, M.: Magnetic characterization of nanocrystalline Ni–Zn ferrite powder prepared by the glyoxylate precursor method. *J Phys D Appl Phys*. **35**, 3035–3040 (2002)
45. Shafi, K.V.P.M., Gedanken, A., Prozorov, R., Balogh, J.: Sonochemical Preparation and Size-Dependent Properties of Nanostructured CoFe₂O₄ Particles. *Chem Mater*. **10**, 3445–3450 (1998)
46. Fu, Y.S., Chen, Q., He, M., Wan, Y., Sun, X., Xia, H., Wang, X.: Copper Ferrite-Graphene Hybrid: A Multifunctional

- Heteroarchitecture for Photocatalysis and Energy Storage. *Ind Eng Chem Res.* **51**, 11700–11709 (2012)
47. Abdellatif, M.H., Innocenti, C., Liakos, I., Scarpellini, A., Marras, S., Salerno, M.: Effect of Jahn-Teller Distortion on the Short Range Magnetic Order in Copper Ferrite. *J Magn Magn Mater.* **424**, 402–409 (2017)
 48. Najmuddin, N., Beitollahi, A., Muhammeda, M., Ansari, N., Devlin, E., Mohseni, S.M., Rezaie, H., Niarchos, D., Akerman, J., Toprak, M.S.: Effect of nanoconfinement on the formation, structural transition and magnetic behavior of mesoporous copper ferrite. *J Alloys Compd.* **598**, 191–197 (2014)
 49. Hankare, P.P., Kadam, M.R., Patil, R.P., Garadkar, K.M., Sasikala, R., Tripathi, A.K.: Effect of zinc substitution on structural and magnetic properties of copper ferrite. *J Alloys Compd.* **501**, 37–41 (2010)
 50. Ahmed, Y.M.Z., Hessien, M.M., Rashad, M.M., Ibrahim, I.A.: Nano-crystalline copper ferrites from secondary iron oxide (mill scale). *J Magn Magn Mater.* **321**, 181–187 (2009)
 51. Pavithradevi, S., Suriyanarayanan, N., Boobalan, T.: Synthesis, structural, dielectric and magnetic properties of polyol assisted copper ferrite nano particles. *J Magn Magn Mater.* **426**, 137–143 (2017)
 52. Rashad, M.M., Mohamed, R.M., Ibrahim, M.A., Ismail, L.F.M., Abdel-Aal, E.A.: Magnetic and catalytic properties of cubic copper ferrite nanopowders synthesized from secondary resources. *Adv Powder Technol.* **23**, 315–323 (2012)
 53. Albuquerque, A.S., Ardisson, J.D., Macedo, W.A.A., López, J.L., Paniago, R., Persiano, A.I.C.: Structure and magnetic properties of nanostructured Ni-ferrite. *J Magn Magn Mater.* **226**, 1379–1381 (2001)
 54. Tolentino, M.V.C., Ardisson, J.D., Moura, F.C.C., Mendonc, R.D., Macedo, W.A.A.: Nanostructured ferrites: Structural analysis and catalytic activity. *Ceram Int.* **38**, 2225–2231 (2012)
 55. Guo, X., Wang, K., Li, D., Qin, J.: Heterogeneous photo-Fenton processes using graphite carbon coating hollow CuFe₂O₄ spheres for the degradation of methylene blue. *Appl Surf Sc.* **420**, 792–801 (2017)
 56. Zhuang, Y.T., GaoW, Y.Y.L., Wang, J.H.: Facile fabrication of three-dimensional porous CuFe₂O₄cages as highly efficient and recyclable heterogeneous catalyst. Magnetically Recoverable Nanocatalysts. *Mater Des.* **130**, 294–301 (2017)